CHIN. PHYS. LETT. Vol. 26, No. 9 (2009) 097302

Electron States in Parallel Double Quantum Dots with a Tunable Inter-Dot Coupling *

CAO Gang(曹刚), LI Hai-Ou(李海欧), TU Tao(涂涛)**, ZHOU Cheng(周诚), HAO Xiao-Jie(郝晓杰), GUO Guang-Can(郭光灿), GUO Guo-Ping(郭国平)***

Key Laboratory of Quantum Information, University of Science and Technology of China, Hefei 230026

(Received 24 April 2009)

We study the electron states on lateral double quantum dots coupled in parallel. The charge stability diagrams are given in terms of the gate voltages of both dots. We discover that the two electron states translate from separated states to coupled states continuously by increasing the inter-dot coupling strength. Our results demonstrate that the parallel-quantum-dot tunability bodes well for future quantum computing applications.

PACS: 73.23.Hk, 03.67.Lx, 73.21.La

Great effort in work on electron spins in semiconductor quantum dots has been taken to enable the physical realization of solid state quantum computation.[1,2] However the single spin states in the quantum dot system are not completely decoupled from the environment.[3] Alternatively, the singlet and triplet states of two electron spins in adjacent double quantum dots are promising candidates for the spin qubit.[4−6] This decoherence free subspace protects the system from collective phase noise due to uniform magnetic field fluctuations.[8,9] In addition, dynamical protection from differential phase noise due to hyperfine interaction with nuclear spins can be implemented within this subspace by means of spin echo technology.[4,10] With these safeguards, a qubit decoherence time approaching microseconds has recently been achieved.[11]

Double semiconductor quantum dots are often referred to as artificial molecules, because these electron boxes allow one to control the number of electrons and their interaction precisely.[12] To control electron states well in double quantum dots, this is one of the most promising platforms for solid state quantum information processing. An important step towards realizing such promise is to generate the molecular quantum states accurately by adjusting the coupling of two quantum dots (artificial atoms). This key element has already been shown in electron transport experiments on two lateral quantum dots coupled in series.[11−13] In contrast, in this Letter we use a different system involving two parallel quantum dots to probe the electron states. The charge stability diagrams are given in terms of the gate voltages of both dots. We observe a continuous transition of two electron states from a separated state exhibiting a square structure to a coupled state exhibiting a honeycomb structure by increasing the inter-dot coupling strength. Our results demonstrate that the parallel quantum dot tunability bodes well for future quantum computing applications.

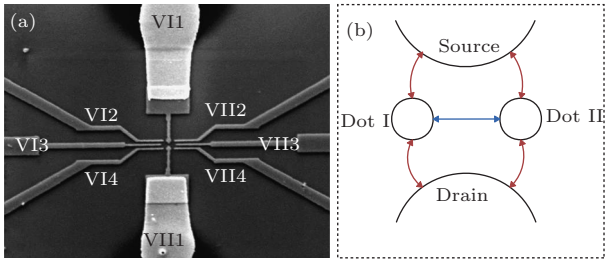


Fig. 1. (a) Scanning electron micrograph of the device. Gates numbered VI1, VI2, VI3, VI4 ,VII1 and VII1, VII2, VII3, VII4, VI1 form the dot I and dot II, respectively, and the lithographic size of each dot is $170 \times 200\,\mathrm{nm}^2$. VI1 and VII1 are used to control the inter-dot coupling strength. To prevent depletion and to enable each lead to simultaneously connect to both dots, a spacer layer of 120-nm-thick polymethyl methacylate (PMMA) was overexposed underneath gates VI1 and VII1 (dark regions). (b) Schematic of the parallel double dot system. Electrons tunnel though the two channels between the public source (S) and drain (D) by applying appropriate gate voltages. The line connecting the two dots indicates the electrons tunneling between the dots.

Sample and Method. Our device was fabricated on a GaAs/$Al_xGa_{1-x}As$ heterostructure containing a two-dimensional electron gas (2DEG) 80 nm below the surface. As determined from the Hall resistance data and Shubnikov-de Haas oscillations in the longitudinal resistance, the electron density is $n = 3.8 \times 10^{11}\,\mathrm{cm}^{-2}$. The sample has a low-temperature mobility $\mu = 9.0 \times 10^5\,\mathrm{cm}^2/\mathrm{V\,s}$, which is high for a 2DEG. As shown in Fig. 1, eight separate metallic gates are configured and operated with tunable gate voltages independently. These gates are designed to

*Supported by the National Basic Research Program of China under Grant Nos 2006CB921900 and 2009CB929600, the Innovation Funds from Chinese Academy of Sciences, and the National Natural Science Foundation of China under Grant Nos 10604052 and 10874163 and 10804104.

**Email: tutao@ustc.edu.cn

***Email: gpguo@ustc.edu.cn

© 2009 Chinese Physical Society and IOP Publishing Ltd

create the potential barriers used to confine the electrons and form the quantum dots, where the lithographic size of each dot is 170 nm × 200 nm. The inter-dot coupling strength can be tuned by the gates Ⅵ1 and Ⅶ1. The device was first immersed into a liquid helium storage dewar at 4.2 K to test the functionality of the gates. The experiment was carried out in an Oxford top-loading dilution refrigerator with base temperature of 15 mK. The standard differential resistance was measured by a quasi-dc lock-in technique using a small ac voltage with 11.3 Hz.

Charge stability diagrams and electron states. Separate characterization of each dot in the closed dot regime yields a standard Coulomb blockade (CB) peak, as shown in Fig. 2(a).[14] In the CB regime, the electrons on the dot are well confined to an integral number and the dot occupancy increases with the gate voltage Ⅵ3 or Ⅶ3. Electron tunneling through the quantum dot is only possible when the charges in the quantum dot change between N and $N+1$. Figure 2(b) shows the differential conductance dI/dV_{sd} versus Ⅵ3 and V_{sd}. Diamond-shaped regions are due to the suppressed current caused by Coulomb Blockade.

To characterize the double quantum dots device and demonstrate its full tunability, in Fig. 3 we show the CB charge diagrams of the conductance versus gates Ⅵ3 and Ⅶ3, as reducing negative voltages on the middle gates Ⅵ1=Ⅶ1 thus increasing the coupling strength between the dots. At weak coupling, the electron states are separated in the nearly independent dots yielding square domain structures in Fig. 3(a). With increasing coupling strength, two electron states are quantum mechanically coupled, i.e., molecular states (tunnel coupling is analogous to bonding). It is clearly seen that from Figs. 3(a)–3(c), the stability diagrams gradually evolve into the honeycomb structures. At large coupling strength the two dots merge into one large dot and the domain boundaries become straight lines in Fig. 3(d).

Theoretical simulations. For better understanding and quantitative comparison with the experimental observations, we perform numerical simulations based on orthodox the Constant Interaction model.[12] Before proceeding, one point need to be clarified: in Ref. [12], only the series double dots were considered. Nevertheless, after direct calculations the formula can be applied to the parallel double quantum dots. The electrochemical potential $\mu_{\rm I}$, $\mu_{\rm II}$ of double dots system can be expressed as

$$\begin{aligned}\mu_{\rm I}(N_{\rm I},N_{\rm II}) &= \Big(N_{\rm I}-\frac{1}{2}\Big)E_{\rm CI}+N_{\rm II}E_{\rm Cm}\\ &\quad-\frac{1}{|e|}(C_{\rm I3}V_{\rm I3}E_{\rm CI}+C_{\rm II3}V_{\rm II3}E_{\rm Cm})+E_{0\rm I},\\ \mu_{\rm II}(N_{\rm I},N_{\rm II}) &= \Big(N_{\rm II}-\frac{1}{2}\Big)E_{\rm CII}+N_{\rm I}E_{\rm Cm}\\ &\quad-\frac{1}{|e|}(C_{\rm II3}V_{\rm II3}E_{\rm CII}+C_{\rm I3}V_{\rm I3}E_{\rm Cm})+E_{0\rm II},\end{aligned}$$

where $N_{\rm I}$ and $N_{\rm II}$ the numbers of electrons in dots I and Ⅱ; $C_{\rm I3}$ and $C_{\rm II3}$ are the gate Ⅵ3, Ⅶ3 capacitances of dots I and Ⅱ; C_m is the corresponding tunneling capacitance between dots I and Ⅱ; $E_{0\rm I}$ and $E_{0\rm II}$ are the single particle ground energies of dots I and Ⅱ, the individual charge energies $E_{\rm CI}$ and $E_{\rm CII}$ of dots I and Ⅱ, and the coupling energy $E_{\rm Cm}$ between dots, which is the change in the energy of one dot when an electron is added to the other dot, can be obtained in terms of the capacitances as

$$E_{\rm CI}=\frac{e^2}{C_{\rm I}}\Big(1-\frac{C_m^2}{C_{\rm I}C_{\rm II}}\Big)^{-1},\ E_{\rm CII}=\frac{e^2}{C_{\rm II}}\Big(1-\frac{C_m^2}{C_{\rm I}C_{\rm II}}\Big)^{-1},$$
$$E_{\rm Cm}=\frac{e^2}{C_m}\Big(\frac{C_{\rm I}C_{\rm II}}{C_m^2}-1\Big)^{-1},$$

where $C_{\rm I}$, $C_{\rm II}$ is the sum of all capacitances attached to dots I and Ⅱ.

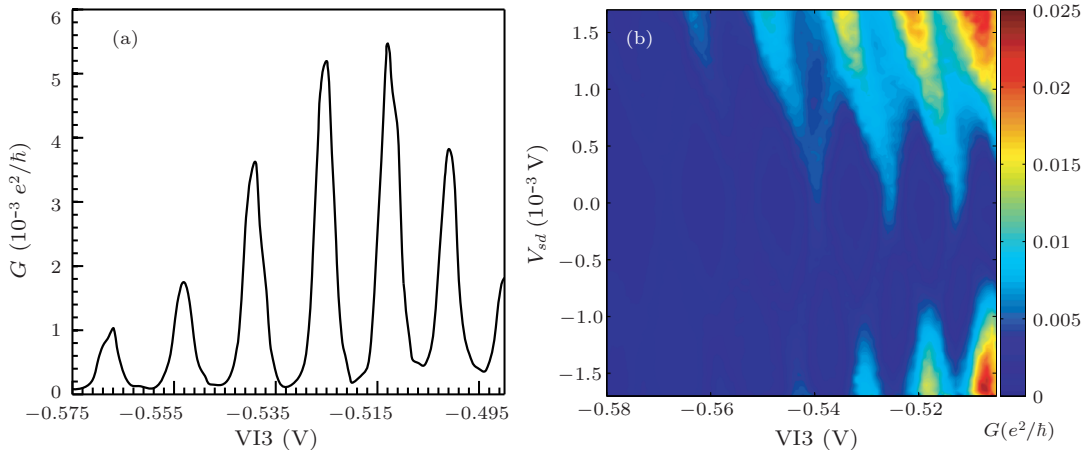


Fig. 2. Transport through dot I. (a) The conductance of dot I as a function of gate voltage Ⅵ3 for source-drain voltage $V_{sd}=0$. (b) The differential conductance versus (Ⅵ3 ,V_{sd}). The diamond-shaped areas around $V_{sd}=0$ are the Coulomb blockade regions where the number of electrons on the dot is fixed. Dot Ⅱ is operated and shows a similar outcome.

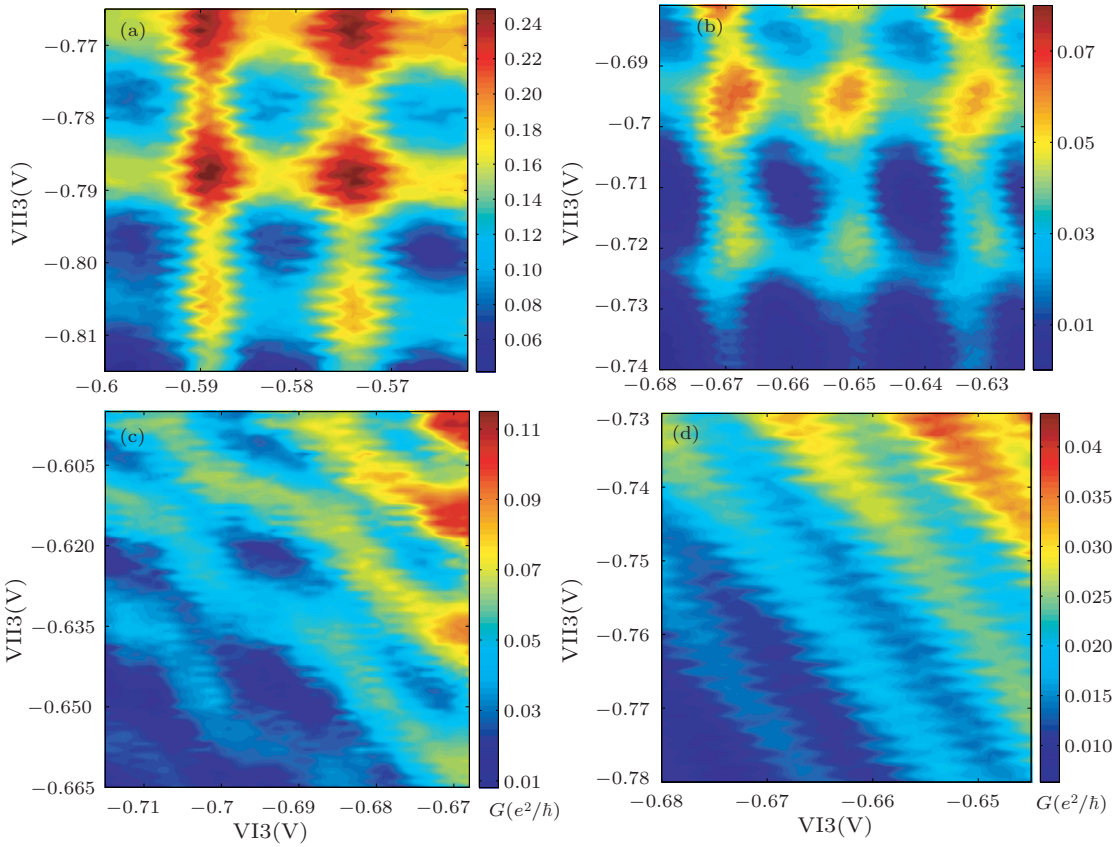


Fig. 3. Experimental plots of stability diagrams of parallel double dots by sweeping VI3 and VII3 with the increasing gate voltages VI1 and VII1. (a) VI1 = VII1 = −0.775 V weak coupling. (b) VI1 = VII1 = −0.770 V and (c) VI1 = VII1 = −0.730 V intermediate coupling. (d) VI4 = VII4 = −0.665 V strong coupling.

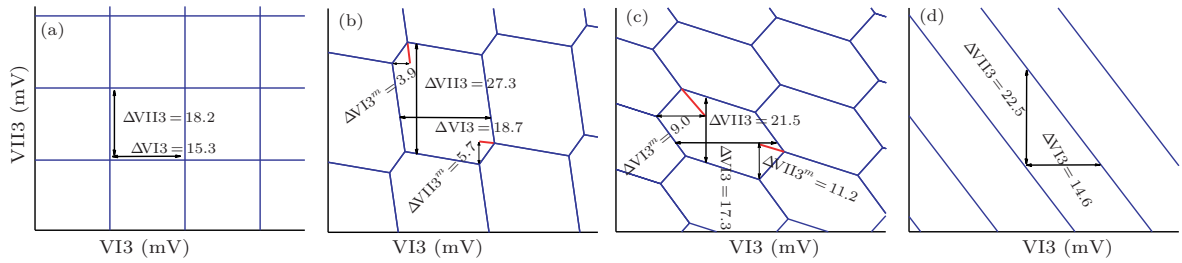


Fig. 4. Theoretical simulations of stability diagrams of parallel double quantum dot system in different inter-dot coupling regimes: (a) weak coupling $C_m/C_{\rm II} = 0$, (b) and (c) intermediate coupling, $C_m/C_{\rm II} = 0.209$, $C_m/C_{\rm II} = 0.521$ and (d) strong coupling, $C_m/C_{\rm II} = 1$. The diagrams are the charging counters using the parameters extracted from Fig. 3. The lines represents the conductance peaks, where the electron will tunnel into or out of the quantum dot and the conductance signals can be observed in the transport measurements.

Double dot system capacitances can be obtained by measuring the sizes and separations of the honeycombs and vertices (Figs. 3(b) and 3(c)).[12] The size of the honeycombs in Fig. 3(b) or 3(c) determines $\Delta V_{\rm I3}$, $\Delta V_{\rm II3}$, where

$$\Delta V_{\rm I3} = \frac{|e|}{C_{I3}}\Big(1 + \frac{\Delta E_{\rm I}}{E_{\rm CI}}\Big), \quad \Delta V_{\rm II3} = \frac{|e|}{C_{\rm II3}}\Big(1 + \frac{\Delta E_{\rm II}}{E_{\rm CII}}\Big).$$

$\Delta E_{\rm I}$, $\Delta E_{\rm II}$ are the level spacing of dots I and II, and $E_{\rm CI}$, $E_{\rm CII}$ can be determined from conductance diamond of each dot in a plot of conductance as a function of V_{sd} and gate voltage. The size of the vertex splitting in Fig. 3(b) or 3(c) determines $\Delta V^m_{\rm I3}$, $\Delta V^m_{\rm II3}$, where

$$\Delta V^m_{\rm I3} = \frac{|e|C_m}{C_{\rm I3}C_{\rm II}}, \quad \Delta V^m_{\rm II3} = \frac{|e|C_m}{C_{\rm II3}C_{\rm I}}.$$

Using the parameters extracted from Fig. 3, the electrochemical potential $\mu_{\rm I}$, $\mu_{\rm II}$ versus the scanning of two gate voltages $V_{\rm I3}$ and $V_{\rm II3}$ for different inter-dot coupling is shown in Fig. 4. The inter-dot coupling strength is characterized by the ratio of tunneling capacitance to total capacitance of each dot, $C_m/C_{\rm I}$ or $C_m/C_{\rm II}$. Depending on the inter-dot coupling strength, the energy profile evolves from a square structure (separated dots, Fig. 4(a), $C_m/C_{\rm II} = 0$), to a honeycomb pattern (intermediate coupling, Fig. 4(b)

$C_m/C_{\text{II}} = 0.209$, Fig. 4(c) $C_m/C_{\text{II}} = 0.521$) then a strip line (strong coupling, Fig. 4(d) $C_m/C_{\text{II}} = 1$, two dots merge into one large dot). These diagrams resemble Fig. 3.

In conclusion, only a few electron transport measurements in double quantum dots coupled in parallel have so far been investigated. Motivated by the relevance of double quantum dot studies for realizing a qubit, we perform a transport experiment on two parallel quantum dots to probe the electron states. By increasing the inter-dot coupling, a continuous transition from a separated two electron state to a coupled two electron state can be observed in the charge stability diagrams, which are consistent with the theoretical simulations. Precise control of the number of electrons in the coupled quantum dot system provides a promising environment for the development of quantum information processing or addressing more complex structures and phenomena.[15]

References

[1] Loss D and DiVincenzo D P 1998 *Phys. Rev.* A **57** 120

[2] Hanson R, Kouwenhoven L P, Petta J R, Tarucha S and Vandersypen L M K 2007 *Rev. Mod. Phys.* **79** 1217

[3] Hanson R and Awschalom D 2008 *Nature* **453** 1043

[4] Taylor J M, Dur W, Zoller P, Yacoby A, Marcus C M and Lukin M D 2005 *Phys. Rev. Lett.* **94** 236803

[5] Taylor J M, Engel H A, Dur W, Yacoby A, Marcus C M, Zoller P and Lukin M D 2005 *Nature Physics* **1** 177

[6] Lin Z R, Guo G P, Tu T, Zhu F Y and Guo G C 2008 *Phys. Rev. Lett.* **101** 230501

[7] Zhu F Y, Hao X J, Tu T, Guo G C and Guo G P 2009 *Chin. Phys. Lett.* **26** 050301

[8] Duan L M and Guo G C 1997 *Phys. Rev. Lett.* **79** 1953

[9] Lidar D A, Chuang I L and Whaley K B 1998 *Phys. Rev. Lett.* **81** 2594

[10] Wu L A and Lidar D A 2002 *Phys. Rev. Lett.* **88** 207902

[11] Petta J R, Johnson A C, Taylor J M, Laird E A, Yacoby A, Lukin M D, Marcus C M, Hanson M P and Gossard A C 2005 *Science* **309** 2180

[12] van der Wiel W G, De Franceschi S and Elzerman J M, Fujisawa T, Tarucha S and Kouwenhoven L P 2003 *Rev. Mod. Phys.* **75** 1

[13] Koppens F H L, Folk J A, Elzerman J M, Hanson R, van Beveren L H W, Vink I T, Tranitz H P, Wegscheider W, Kouwenhoven L P and Vandersypen L M K 2005 *Science* **309** 1346

[14] Marcus C M, McEuen P L, Tarucha S, Westervelt R M and Wingreen N 1997 *NATO ASI Conference Proceedings* ed Sohn L L, Kouwenhoven L P and Schon G (Kluwer, Dordrecht)

[15] Lv R and Liu Z R 2007 *Chin. Phys. Lett.* **24** 195